

Article

Intracluster Sulphur Dioxide Oxidation by Sodium Chlorite Anions: A Mass Spectrometric Study

Chiara Salvitti *, Federico Pepi , Anna Troiani * and Giulia de Petris

Dipartimento di Chimica e Tecnologie del Farmaco, "Sapienza" University of Rome, 00185 Rome, Italy; federico.pepi@uniroma1.it (F.P.); giulia.depetris@uniroma1.it (G.d.P.)

* Correspondence: chiara.salvitti@uniroma1.it (C.S.); anna.troiani@uniroma1.it (A.T.)

Abstract: The reactivity of $[\text{NaL}\cdot\text{ClO}_2]^-$ cluster anions ($\text{L} = \text{ClO}_x^-$; $x = 0-3$) with sulphur dioxide has been investigated in the gas phase by ion–molecule reaction experiments (IMR) performed in an in-house modified Ion Trap mass spectrometer (IT-MS). The kinetic analysis revealed that SO_2 is efficiently oxidised by oxygen-atom (OAT), oxygen-ion (OIT) and double oxygen transfer (DOT) reactions. The main difference from the previously investigated free reactive ClO_2^- is the occurrence of intracluster OIT and DOT processes, which are mediated by the different ligands of the chlorite anion. This gas-phase study highlights the importance of studying the intrinsic properties of simple reacting species, with the aim of elucidating the elementary steps of complex processes occurring in solution, such as the oxidation of sulphur dioxide.

Keywords: cluster reactivity; sulphur dioxide; sodium chlorite; mass spectrometry; ion-molecule reactions; oxidation reactions



Citation: Salvitti, C.; Pepi, F.; Troiani, A.; de Petris, G. Intracluster Sulphur Dioxide Oxidation by Sodium Chlorite Anions: A Mass Spectrometric Study. *Molecules* **2021**, *26*, 7114. <https://doi.org/10.3390/molecules26237114>

Academic Editor: Giorgio S. Senesi

Received: 3 November 2021

Accepted: 22 November 2021

Published: 24 November 2021

Publisher's Note: MDPI stays neutral with regard to jurisdictional claims in published maps and institutional affiliations.



Copyright: © 2021 by the authors. Licensee MDPI, Basel, Switzerland. This article is an open access article distributed under the terms and conditions of the Creative Commons Attribution (CC BY) license (<https://creativecommons.org/licenses/by/4.0/>).

1. Introduction

Pollution and other environmental issues are typically associated with the atmospheric emissions of exhaust flue gases produced by power plants and industries [1]. Different technologies, collectively known as flue gas cleaning processes, attempt to mitigate the release of greenhouse gases deriving from the burning of coal to generate electrical power [2]. Most efforts in this field are aimed at planning pollutant-control strategies to reduce sulphur dioxide which is referred to as the main precursor of acid rainfalls and atmospheric particulate [3–5]. To this end, the European Union established the 2016/2284/UE Regulation that intends to progressively reduce SO_2 emissions until 2029 and for the next few years [6].

Among the flue gas desulphurization (FGD) methods, the wet scrubbing system is a low-cost and simple technology based on the reaction between SO_2 and an alkaline sorbent, typically limestone [7–9]. Although engineers mostly design separate air-cleaning devices for individual gas emission removal, the search for multi-pollutant control systems would reduce the need for large installation areas and operation costs [10]. To this end, sodium chlorite (NaClO_2) is one of the most effective reagents for the simultaneous removal of oxides of sulphur (SO_x) and nitrogen (NO_x) [11]. The addition of this compound to seawater solution has been recently exploited to improve the elimination of SO_2 and favour the development of environmentally friendly seawater-based FGD [12].

The strong oxidative properties of NaClO_2 allows the conversion of sulphites (SO_3^{2-}) produced by SO_2 absorption to the harmless sulphates (SO_4^{2-}) that are easily solubilized in water and thus removed [13,14]. Nevertheless, many factors can affect the outcome of the scrubbing process (e.g., pH, temperature, oxidant concentration, oxidant/gas contact time, volumetric gas, liquid flow rates) and the influence of these parameters has to be carefully evaluated in the design of the operating systems [15–17]. For instance, solution salinity is known to increase SO_2 absorption efficiency, and under alkaline conditions needed for $\text{SO}_2/\text{SO}_3^-$ conversion, the occurrence of a gas-solid interface reaction between SO_2 and NaClO_2 gives rise to the formation of Cl^\cdot , ClO^\cdot and OCIO^\cdot chlorinated species which may

enhance the concomitant NO oxidation in multi-pollutant removal plants [18,19]. On the other side, the above-mentioned factors can contribute to masking the intrinsic reactivity of NaClO₂ towards sulphur dioxide preventing the elucidation of the mechanistic details that lead to the oxidation of SO₂ and the formation of collateral products.

A successful strategy to avoid solution interfering effects and investigate the chemical processes at a strictly molecular level consists in performing gas-phase studies by mass spectrometry [20–26]. This technique is one of the most routinely employed for analytical purposes in a plethora of research fields spanning, *inter alia*, from foods and drugs to biology [27–34] or from geology to atmospheric chemistry [35–39]. Less well known is the use of mass spectrometry in fields such as catalysis, nevertheless, in the last years, mass spectrometry has been widely employed to assess the elementary steps of a chemical transformation by unravelling mechanistic pathways and elucidating the factors which affect the reaction outcome [40–46]. Accordingly, ion-molecule reaction (IMR) experiments were largely intended to investigate the reactivity of ionic reagents generated at their ground state towards neutral species under single-collision conditions. The gas-phase reaction of free ClO[−] and ClO₂[−] anions towards SO₂ has actually provided important information on the intrinsic properties of naked chlorite leading to the oxidation of sulphur dioxide to SO₃, SO₃^{·−} and SO₄^{·−}, with the concomitant formation of the chlorinated species ClO[−], ClO[·], and Cl[·] [47]. These reaction channels, respectively referred to as oxygen-atom (OAT), oxygen-ion (OIT), and double oxygen transfer (DOT), may represent simplified models of large-scale reactions occurring in the atmosphere or involved in the flue-gas desulphurization processes.

In addition, electrospray ionization mass spectrometry has been long-time devoted to the study of salt speciation [48–50] showing its capability in controlling the size and charge of cluster ions. As a result, ionic clusters can be considered miniaturized systems to investigate the intrinsic features of matter aggregation phenomena [51,52]. Accordingly, the study of the gas-phase reactions of SO₂ with positive and negative carbonate cluster ions contributed to highlighting the major role of the charge in the kinetics of smallest clusters, as well as the different reactivity when charged cluster are ligated to a NaOH molecule [53]. Indeed, a point-charge ligand can generate oriented external electric fields able to change thermodynamics and kinetics of a gas-phase thermal process by controlling the reaction mechanism, efficiencies, and product distribution [54–56].

Continuing with our studies focused on the chemistry of sulphur dioxide [57–62], here we report on the gas-phase reactivity of negatively charged chlorite cluster ions, [NaL·ClO₂][−] (L = ClO_x[−] with *x* = 0–3), towards SO₂ investigated by ion-molecule reaction experiments. In this way, the effect of the ligation of a neutral molecule to ClO₂[−] that changes the ion size and charge distribution of the cluster has been evaluated based on the known reactivity of naked ClO₂[−] species with SO₂.

2. Results and Discussion

Oxo-halogenated ions investigated in this work were generated by the negative electrospray ionization of NaClO₂ solutions typically yielding a series of singly-charged cluster ions in which NaClO₂ is clustered to the ClO₂[−] anion to form aggregates resembling the general formula [(NaClO₂)_{*n*}·ClO₂][−], *n* varying from 1 to 4 in the *m/z* range 100–500 (Figure S1). Aggregation phenomena are indeed characteristic of electrosprayed saline compounds [49] and are influenced by the solute concentrations and source parameters [53]. Furthermore, the electric field applied between the capillary and the skimmer plate accounts for the occurrence of electrochemical reactions at the conductive contact-solution interface near the ES emitter [63]. The detection of ClO_x[−] (*x* = 0, 1, 3) anions in addition to the ClO₂[−] parent species suggests the effective occurrence of in-source redox processes. For *x* = 1 and 3, the corresponding ClO[−] and ClO₃[−] anions do not undergo significant aggregation phenomena. On the contrary, Cl[−] anions promote aggregation with NaClO₂ to form [(NaClO₂)_{*n*}·Cl][−] ions (*n* = 1–5), and mixed clusters of general formula [Na_{*x*}Cl_{*y*}O_{*z*}][−] were also identified as minor species, as shown in the Supplementary Materials (Figure S1).

The simplest ClO_2^- clusters for $n = 1$ were found at m/z 125 and 157 and respectively attributed to the ^{35}Cl isotopologue of $[\text{NaCl}\cdot\text{ClO}_2]^-$ and $[\text{NaClO}_2\cdot\text{ClO}_2]^-$ species. The assignment was based on the distinctive $^{35/37}\text{Cl}$ isotope pattern and on the corresponding collision-induced dissociation (CID) mass spectra. The ion $[\text{Na}^{35}\text{Cl}\cdot^{35}\text{ClO}_2]^-$ at m/z 125 predominantly fragments by losing a Na^{35}Cl neutral counterpart giving rise to the $^{35}\text{ClO}_2^-$ daughter ion at m/z 67 (Figure 1a). The gas-phase decomposition of the corresponding $^{35/37}\text{Cl}$ isotopomer (m/z 127) predictably leads to the formation of an equal ratio of $^{35}\text{ClO}_2^-$ and $^{37}\text{ClO}_2^-$ fragments at m/z 67 and 69, respectively (Figure 1b). The parent ion can be therefore described as a complex of the type $[\text{Cl}\cdot\text{Na}\cdot\text{ClO}_2]^-$ in which both the chloride (Cl^-) and chlorite (ClO_2^-) anions are coordinated to the sodium cation (Na^+). In particular, the chlorite moiety is reasonably consistent with an OClO^- species rather than with the more stable ClOO^- isomer, the presence of which can be excluded considering the structure of the precursor salt, NaClO_2 , and the high energy barrier to the isomerization, calculated to be $51.1 \text{ kcal}\cdot\text{mol}^{-1}$, [47] which cannot be overcome by the ions during the ionization process.

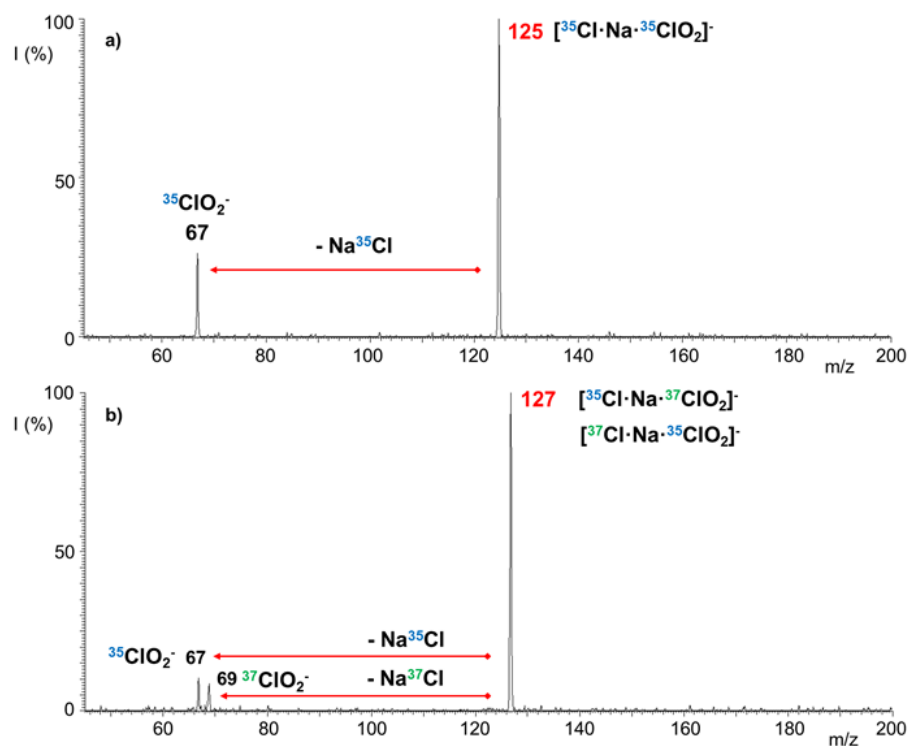


Figure 1. ESI(-) CID mass spectra of the isolated (a) $[\text{Na}^{35}\text{Cl}\cdot^{35}\text{ClO}_2]^-$ at m/z 125 and (b) $[\text{Na}^{35}\text{Cl}\cdot^{37}\text{ClO}_2]^-$ and $[\text{Na}^{37}\text{Cl}\cdot^{35}\text{ClO}_2]^-$ at m/z 127.

Similarly, the CID mass spectrum of the ionic species $[\text{Na}^{35}\text{ClO}_2\cdot^{35}\text{ClO}_2]^-$ at m/z 157 shows the only daughter ion $^{35}\text{ClO}_2^-$ at m/z 67, arising from the loss of a NaClO_2 neutral counterpart (Figure 2a). Accordingly, the gas-phase decomposition of the isotopomer at m/z 159 leads to the formation of an equal ratio of $^{35}\text{ClO}_2^-$ and $^{37}\text{ClO}_2^-$ fragment ions at m/z 67 and 69 (Figure 2b), accounting for the symmetrical complex $[\text{ClO}_2\cdot\text{Na}\cdot\text{ClO}_2]^-$.

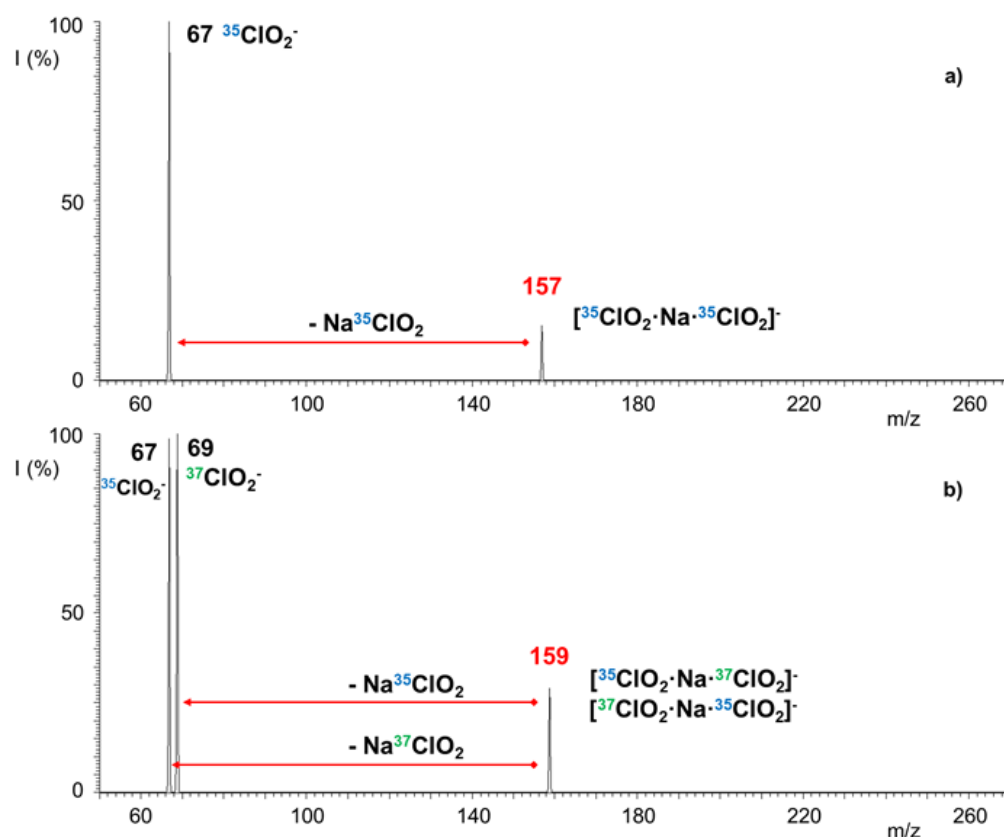
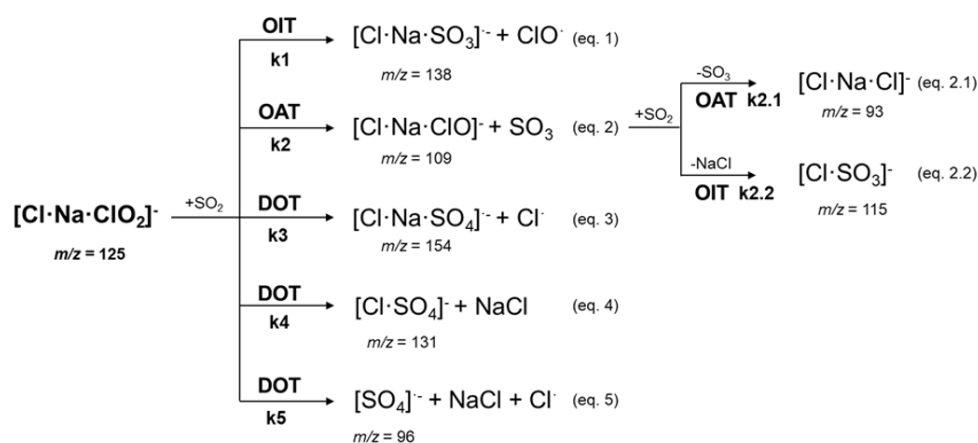


Figure 2. ESI(-) CID mass spectra of the isolated (a) $[\text{Na}^{35}\text{ClO}_2 \cdot ^{35}\text{ClO}_2]^-$ at m/z 157 and (b) $[\text{Na}^{35}\text{ClO}_2 \cdot ^{37}\text{ClO}_2]^-$ and $[\text{Na}^{37}\text{ClO}_2 \cdot ^{35}\text{ClO}_2]^-$ at m/z 159.

Each ionic species described above was in turn isolated into the ion trap and exposed to unreactive gas (He) over long accumulation times. Since no remarkable signal loss occurred, these ions can be considered rather stable gaseous chlorine-based aggregates. When reacted with SO_2 , they showed a noteworthy reactivity. In the following, the reactivity of selected cluster ions, $[\text{Cl} \cdot \text{Na} \cdot \text{ClO}_2]^-$ and $[\text{ClO}_2 \cdot \text{Na} \cdot \text{ClO}_2]^-$, will be described in depth, starting from the simplest $[\text{Cl} \cdot \text{Na} \cdot \text{ClO}_2]^-$. At the occurrence, the formula of the reacting species is written with the sodium cation in the centre, to highlight the reactive anionic units. Similar to the reactions observed with the non-clustered ClO_2^- ions [47], both $[\text{Cl} \cdot \text{Na} \cdot \text{ClO}_2]^-$ and $[\text{ClO}_2 \cdot \text{Na} \cdot \text{ClO}_2]^-$ cluster ions promote oxygen-atom transfer (OAT), oxygen-ion transfer (OIT), and double oxygen transfer (DOT) towards SO_2 . The main difference with the free ClO_2^- is that when SO_2 is oxidised, the oxidised products predominantly remain in the cluster and are not released as free species. Accordingly, the whole mechanistic picture of the reactions between $[\text{Cl} \cdot \text{Na} \cdot \text{ClO}_2]^-$ and $[\text{ClO}_2 \cdot \text{Na} \cdot \text{ClO}_2]^-$ anions towards SO_2 was outlined by identifying direct and consecutive pathways, measuring the rate constants for each reaction channel, and structurally characterizing the ionic products by CID experiments.

2.1. Reactivity of $[\text{Cl} \cdot \text{Na} \cdot \text{ClO}_2]^-$ Cluster Anion

$[\text{Cl} \cdot \text{Na} \cdot \text{ClO}_2]^-$ cluster anions react with SO_2 at room temperature giving rise to the products shown in Scheme 1, through a complex series of parallel and consecutive reactions. A kinetic plot showing the time progress of the reaction is displayed in Figure 3. The identity of the ionic products from reactions 1–5 has been probed by collision-induced dissociation as discussed in the following. As reported in Table 1, the reaction of $[\text{Cl} \cdot \text{Na} \cdot \text{ClO}_2]^-$ has a rate constant (k_{dec}) of 2.88×10^{-10} ($\pm 30\%$) $\text{cm}^3 \text{s}^{-1} \text{mol}^{-1}$ and an efficiency (k/k_{coll}) of 24.2%.



Scheme 1. Reactivity scheme $[\text{Cl}\cdot\text{Na}\cdot\text{ClO}_2]^-$ ions ($m/z = 125$) with SO_2 . Oxygen transfer channels (OIT, OAT, DOT) and bimolecular rate constants are indicated for each reaction.

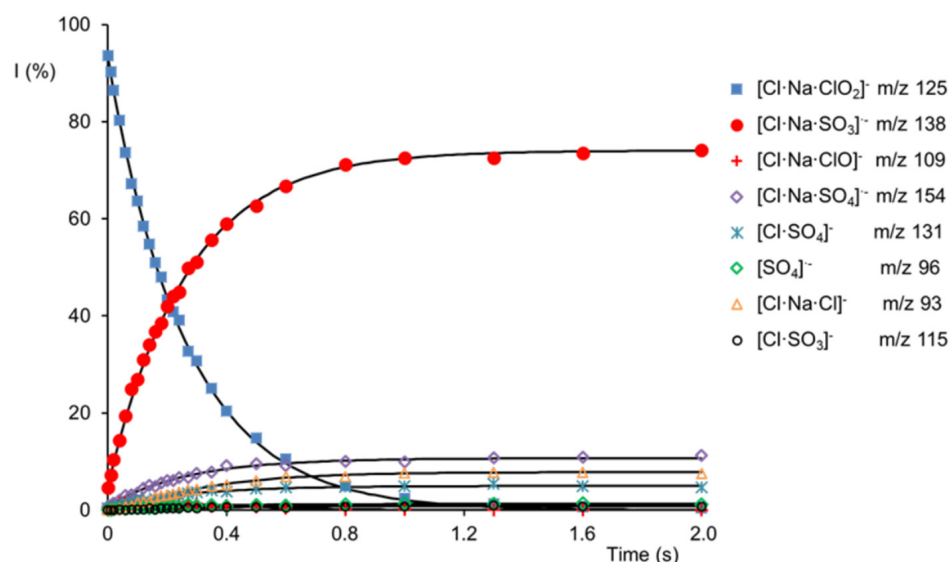


Figure 3. Kinetic plot and best fit lines of the reaction of isolated $[\text{NaCl}\cdot\text{ClO}_2]^-$ ions ($m/z = 125$) with SO_2 . $P_{\text{SO}_2} = 5.26 \times 10^{-7}$ Torr. ■ $[\text{Cl}\cdot\text{Na}\cdot\text{ClO}_2]^-$ ($m/z = 125$) ($R^2 = 0.9991$); ● $[\text{Cl}\cdot\text{Na}\cdot\text{SO}_3]^-$ ($m/z = 138$) ($R^2 = 0.9986$); + $[\text{Cl}\cdot\text{Na}\cdot\text{ClO}]$ ($m/z = 109$) ($R^2 = 0.9770$); ◇ $[\text{Cl}\cdot\text{Na}\cdot\text{SO}_4]^-$ ($m/z = 154$) ($R^2 = 0.9915$); × $[\text{Cl}\cdot\text{SO}_4]^-$ ($m/z = 131$) ($R^2 = 0.9868$); ◇ $[\text{SO}_4]^-$ ($m/z = 96$) ($R^2 = 0.9846$); △ $[\text{Cl}\cdot\text{Na}\cdot\text{Cl}]$ ($m/z = 93$) ($R^2 = 0.9946$); ○ $[\text{Cl}\cdot\text{SO}_3]^-$ ($m/z = 115$) ($R^2 = 0.9946$).

Although the larger size of $[\text{Cl}\cdot\text{Na}\cdot\text{ClO}_2]^-$ is predictably responsible for the decrease of the overall reaction rate compared to that of naked ClO_2^- (2.88 vs. $9.10 \times 10^{-10} \text{ cm}^3 \text{ s}^{-1} \text{ mol}^{-1}$), the intrinsic reactivity of the two ionic species is comparable, except for small differences in the branching ratios of the three oxygen transfer reactions. For the sake of clarity, the reactivity, OIT, OAT and DOT, is indicated in each reaction channel.

Table 1. Rate constants ($\text{cm}^3 \text{s}^{-1} \text{mol}^{-1}$), branching ratios ($\% \Sigma$) and efficiencies (k/k_{coll}) for the reactions of $[\text{L} \cdot \text{M} \cdot \text{ClO}_2]^-$ ($\text{L} = \text{Cl, F, Br, I, ClO}_2, \text{SO}_3$; $\text{M} = \text{Na, Li}$) anions with SO_2 . The reaction of ClO_2^- with SO_2 is also reported for comparative purposes. OIT: oxygen ion transfer; OAT: oxygen atom transfer; DOT: double oxygen transfer.

Reaction	$k_{\text{dec}} (\times 10^{-10})^{\S}$	$k/k_{\text{coll}} (\%)$	OIT	OAT	DOT
$\text{ClO}_2^- + \text{SO}_2$ [47]	9.10	63.8	86.5	4.2	9.3
$[\text{Cl} \cdot \text{Na} \cdot \text{ClO}_2]^- + \text{SO}_2$	2.88	24.2	74.2	8.8	17.0
$[\text{F} \cdot \text{Na} \cdot \text{ClO}_2]^- + \text{SO}_2$	3.75	30.8	89.2	3.7	7.1
$[\text{Br} \cdot \text{Na} \cdot \text{ClO}_2]^- + \text{SO}_2$	2.12	18.7	73.4	10.1	16.5
$[\text{I} \cdot \text{Na} \cdot \text{ClO}_2]^- + \text{SO}_2$	1.85	16.8	68.9	13.7	17.4
$[\text{Cl} \cdot \text{Li} \cdot \text{ClO}_2]^- + \text{SO}_2$	1.81	14.5	84.7	7.9	7.4
$[\text{ClO}_2 \cdot \text{Na} \cdot \text{ClO}_2]^- + \text{SO}_2$	7.48	66.0	81.8	4.8	13.4
$[\text{SO}_3 \cdot \text{Na} \cdot \text{ClO}_2]^- + \text{SO}_2$	3.74	33.0	70.4	6.9	22.7
$[(\text{NaClO}_2)_2 \cdot \text{ClO}_2]^- + \text{SO}_2$	7.39	68.1	-	-	-

$^{\S} \pm 30\%$.

The main reaction of $[\text{Cl} \cdot \text{Na} \cdot \text{ClO}_2]^-$ leads to the formation of the ionic product $[\text{Cl} \cdot \text{Na} \cdot \text{SO}_3]^-$ at m/z 138 and a ClO^\bullet radical species (Equation (1)). The reaction proceeds quickly with a rate constant k_1 of $2.13 \times 10^{-10} (\pm 30\%) \text{cm}^3 \text{s}^{-1} \text{mol}^{-1}$ (Table 2), and a branching ratio of 74.2% (Table 1). The collision-induced dissociation of the product ion at m/z 138 gives rise to the SO_3^- ion at $m/z = 80$ (Figure S3) through the loss of a neutral NaCl consistent with a $[\text{Cl} \cdot \text{Na} \cdot \text{SO}_3]^-$ connectivity, hinting at the occurrence of an intracuster oxidation of SO_2 to SO_3^- through an oxygen ion transfer (OIT) process.

Table 2. Rate constants ($\text{cm}^3 \text{mol}^{-1} \text{s}^{-1}$) for the reactions of the $[\text{Cl} \cdot \text{Na} \cdot \text{ClO}_2]^-$ anion with SO_2 . OIT: oxygen ion transfer; OAT: oxygen atom transfer; DOT: double oxygen transfer.

Reactivity	$k \times 10^{-10} \text{cm}^3 \text{mol}^{-1} \text{s}^{-1}^{\S}$		
OIT	k_1	$k_{2,2}$	
	2.13	0.743	
OAT	k_2	$k_{2,1}$	
	0.251	7.53	
DOT	k_3	k_4	k_5
	0.306	0.147	0.034

$^{\S} \pm 30\%$.

Furthermore, $[\text{Cl} \cdot \text{Na} \cdot \text{SO}_3]^-$ was found to be unreactive towards SO_2 thus confirming the presence of the two notoriously inert Cl^- and SO_3^- moieties [47]. The Cl^- anion only plays a spectator role, whereas the sodium cation is reasonably involved in the coordination of both Cl^- and SO_3^- anions.

A minor channel gives rise to $[\text{Cl} \cdot \text{Na} \cdot \text{ClO}]^-$ at m/z 109 and SO_3 (Equation (2)), with a rate constant k_2 of $2.51 \times 10^{-11} (\pm 30\%) \text{cm}^3 \text{s}^{-1} \text{mol}^{-1}$ (Table 2), and a branching ratio of 8.8% (Table 1). The product ion $[\text{Cl} \cdot \text{Na} \cdot \text{ClO}]^-$ at m/z 109 resembles an aggregate in which a Cl^- spectator anion and a ClO^- moiety are both coordinated to sodium cation, as evidenced by its CID mass spectrum. Through this path, SO_2 is therefore oxidised to SO_3 by an oxygen atom transfer (OAT) reaction. Once formed, $[\text{Cl} \cdot \text{Na} \cdot \text{ClO}]^-$ displays the distinctive reactivity of the surrounding ClO^- moiety towards SO_2 [47] that consists in a further SO_2 to SO_3 conversion (Equation (2.1)), through a second OAT process, and in an intracuster reaction giving $[\text{Cl} \cdot \text{SO}_3]^-$ at $m/z = 115$ through an OIT process (Equation (2.2)). The rate constants of the two competitive processes are respectively $k_{2,1} = 7.53 \times 10^{-10} (\pm 30\%)$ and $k_{2,2} = 7.43 \times 10^{-11} (\pm 30\%) \text{cm}^3 \text{s}^{-1} \text{mol}^{-1}$ (Table 2). Not surprisingly, the OAT undergone by $[\text{Cl} \cdot \text{Na} \cdot \text{ClO}_2]^-$ (Equation (2)) is slower with respect to the same process undergone by $[\text{Cl} \cdot \text{Na} \cdot \text{ClO}]^-$ (Equation (2.1)), reflecting the different reactivity of the free

ClO_2^- and ClO^- species [47]. The first preferably oxidises SO_2 through an OIT process, whereas the OAT is faster in the case of ClO^- .

Finally, the $[\text{Cl}\cdot\text{Na}\cdot\text{ClO}_2]^-$ parent ion is involved in different reactions collectively responsible for a double oxygen transfer (DOT) to SO_2 with the formation of product ions containing a sulphate anion, $\text{SO}_4^{\cdot-}$ (Equations (3)–(5)). The sulphate moiety can be either found as a clustered ion, as in Equations (3) and (4), or it can be a free anion as in Equation (5). In Reactions (3) and (4), upon the oxidation of SO_2 to $\text{SO}_4^{\cdot-}$, a NaCl or Cl^\cdot neutral moieties are respectively released. In any case, it is formed through an overall O_2^- transfer and the DOT processes account for a branching ratio of 17.0% (Table 1).

The ionic product at m/z 154 (Equation (3)) is consistent with a $[\text{Cl}\cdot\text{Na}\cdot\text{SO}_4]^-$ structure according to its fragmentation into $\text{SO}_4^{\cdot-}$ ion at $m/z = 96$ (Figure S4) and loss of the neutral NaCl . The reaction occurs with a rate constant k_3 of 3.06×10^{-11} ($\pm 30\%$) $\text{cm}^3 \text{s}^{-1} \text{mol}^{-1}$ and represents the main DOT path. Alternatively, the $\text{SO}_4^{\cdot-}$ moiety can remain attached to the Cl^\cdot radical, and releasing a NaCl moiety leads to the product ion $[\text{Cl}\cdot\text{SO}_4]^-$ at m/z 131 with a k_4 of 1.47×10^{-11} ($\pm 30\%$) $\text{cm}^3 \text{s}^{-1} \text{mol}^{-1}$ (Equation (4)). According to the electron affinity values for SO_4 (EA = 5.10 eV) and Cl (EA = 3.61 eV) [64], the negative charge of the $[\text{Cl}\cdot\text{SO}_4]^-$ product ion is mostly located on the SO_4 moiety, as confirmed by the dissociation of this cluster into $\text{SO}_4^{\cdot-}$ ion at $m/z = 96$ (Figure S5).

Finally, $\text{SO}_4^{\cdot-}$ is also generated as a free ion through reaction 5 with a k_5 of 3.4×10^{-12} ($\pm 30\%$) $\text{cm}^3 \text{s}^{-1} \text{mol}^{-1}$. Not surprisingly, the free $\text{SO}_4^{\cdot-}$ ion is the least abundant product formed through the DOT paths. In the clustered species, $[\text{Cl}\cdot\text{SO}_4]^-$ and $[\text{Cl}\cdot\text{Na}\cdot\text{SO}_4]^-$, the negative charge can be more favourably dispersed in larger species.

The comparison with the reactivity of the free ClO_2^- anion shows that also with the $[\text{Cl}\cdot\text{Na}\cdot\text{ClO}_2]^-$ clustered anions the OIT remains the main reaction channel. When ClO_2^- was reacted with SO_2 , the small differences in the electron affinities between ClO^- (EA of 2.27 eV) and SO_3 (EA of 2.06 eV) [64] only resulted in close energies (-24.6 and $-25.6 \text{ kcal mol}^{-1}$) calculated for the two alternative exit channels, namely $\text{SO}_3^{\cdot-} (+\text{ClO}^\cdot)$ and $\text{SO}_3 (+\text{ClO}^-)$ [47]; therefore, the prevalence of the OIT process was attributed to kinetic factors. Contrarywise, thermochemical factors favoured the OAT reaction over the OIT process in the reactivity of the free ClO^- anion with SO_2 due to the significantly higher electron affinity of Cl (EA = 3.61 eV) with respect to that of SO_3 (EA = 2.06 eV). Accordingly, in the reactivity of $[\text{Cl}\cdot\text{Na}\cdot\text{ClO}]^-$ ion, OAT (Equation (2.1)) prevails over the OIT process (Equation (2.2)) by a ratio of ca. 10/1. The in-depth theoretical analyses performed on the free ClO_2^- species [47] can also give some insights into the reactivity observed with the clustered chlorite anions. The potential energy surface (PES) of $[\text{OClO}\cdot\text{SO}_2]^-$ system, was characterised by an early transition state that accounts for the almost barrierless formation of $\text{SO}_3^{\cdot-}$. In the TS, the negative charge is exclusively located on the preformed SO_3 group ($1.02 e^-$), that is prone to rapid dissociation into the sulphite radical anion, and that strongly competes with the OAT and DOT processes. The formation of SO_3 and $\text{SO}_4^{\cdot-}$ occurs through common intermediates, found on the double well PES, which dissociate reflecting the endothermicity of the two processes. This theoretical analysis is well suited to also explain the reactivity observed for the ligated $[\text{Cl}\cdot\text{Na}\cdot\text{ClO}_2]^-$ cluster ions with SO_2 , and that of the other ligated species described in the following sections. The NaCl ligand does not affect the outcome of the oxidation reactions. Rather, it seems to have the effect of spreading the charge on the cluster, eventually lowering the reaction rate.

Overall, an increase of DOT and OAT processes at the expense of OIT channel is evidenced for the $[\text{Cl}\cdot\text{Na}\cdot\text{ClO}_2]^-$ cluster ion with respect to the non-clustered ClO_2^- anion.

Effect of the Ligand

To deeply investigate the role of the NaCl ligand in the reactivity of $[\text{Cl}\cdot\text{Na}\cdot\text{ClO}_2]^-$ ion towards SO_2 , Cl^- was first replaced by X^- anion ($\text{X} = \text{F}, \text{Br}, \text{I}$) to form the corresponding $[\text{X}\cdot\text{Na}\cdot\text{ClO}_2]^-$ reactive species and subsequently Li^+ was inserted in place of Na^+ to evaluate the role of the cation. Only non-redox-active ligands were used in order to make a

comparison with the effect of salinity in solution, where it is known that the increase in ionic strength determines an increase in the absorption efficiency of SO_2 , [18].

As reported in Table 1, the overall rate constant (k_{dec}) increases with the charge density of X anion, reaching the highest value of 3.75×10^{-10} ($\pm 30\%$) $\text{cm}^3 \text{s}^{-1} \text{mol}^{-1}$ with the smallest F anion (ion radius = 136 pm) and the lowest value of 1.85×10^{-10} ($\pm 30\%$) $\text{cm}^3 \text{s}^{-1} \text{mol}^{-1}$ with the largest I anion (ion radius = 216 pm) (Table 1) [65].

Regarding the branching ratios of the three reaction channels, $[\text{I}\cdot\text{Na}\cdot\text{ClO}_2]^-$ and $[\text{Br}\cdot\text{Na}\cdot\text{ClO}_2]^-$ show a reactivity distribution comparable to that of the $[\text{Cl}\cdot\text{Na}\cdot\text{ClO}_2]^-$ ion. On the contrary, an increase of the OIT process at the expense of the OAT and DOT channels was reported for $[\text{F}\cdot\text{Na}\cdot\text{ClO}_2]^-$ cluster species. As a consequence of the high charge density on the fluoride ion, the $[\text{F}\cdot\text{Na}\cdot\text{SO}_3]^-$ ionic product arising from the OIT process adds an SO_2 molecule giving rise to a labile adduct of the type $[\text{F}\cdot\text{Na}\cdot\text{SO}_3\cdot\text{SO}_2]^-$ never observed with the other reactant ions. The OAT process increases down the halogen series, whereas the opposite occurs with the OIT process.

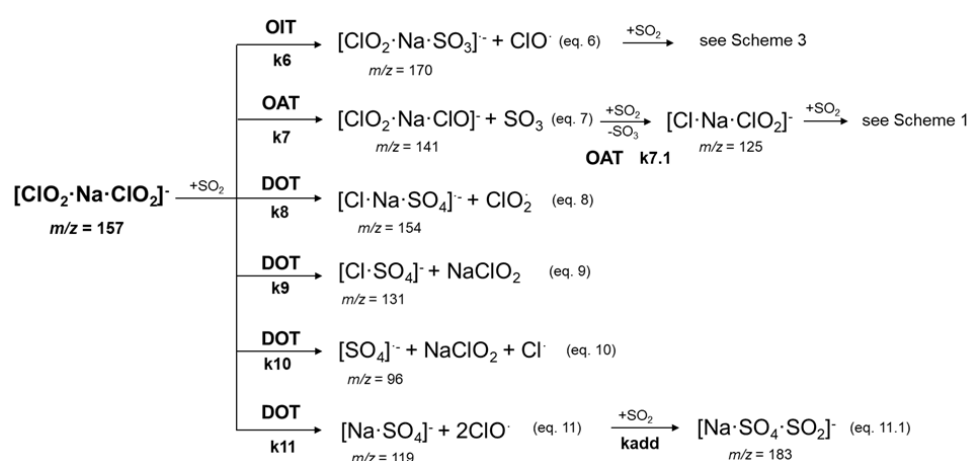
Passing to the cation effect, an opposite trend was observed, as the reaction rate decreases by increasing the positive charge density on the metal. The overall rate constant for the $[\text{Cl}\cdot\text{Li}\cdot\text{ClO}_2]^- + \text{SO}_2$ reaction is indeed almost three times lower than the corresponding value for the $[\text{Cl}\cdot\text{Na}\cdot\text{ClO}_2]^- + \text{SO}_2$ system, highlighting the central role of an external electric field in modelling the reaction kinetics. [54–56] Minor effect of the charge density is instead reported for the general reactivity scheme of $[\text{Cl}\cdot\text{Li}\cdot\text{ClO}_2]^-$ anion.

The main role played by the different ligands described above might be due to the spreading the negative charge of ClO_2^- within the cluster, the effect of which is reflected in the oxidative capacity of ClO_2^- ion: the higher the charge density of the ligand, the faster the reaction. Passing from F^- to I^- , the former forms a tighter ion pair with Na^+ , making the chlorite anion more available to oxidise sulphur dioxide. A second effect concerns the steric hindrance to the approach of SO_2 due to the neutral ligand, whereby ligands of larger dimensions lead to a decrease in the overall reaction rate. An opposite effect is observed with the lithium cation, whose small size increases the interactions with both Cl^- and ClO_2^- , reducing the oxygen transfer rate of the latter. The effect of the non-redox ligands here tested is different to that played in solution, where an increase in ionic strength (i.e., the salinity) has the effect of increasing the SO_2 absorption efficiency by the solutions and therefore the overall efficiency of wet scrubbing processes [18].

2.2. Reactivity of $[\text{ClO}_2\cdot\text{Na}\cdot\text{ClO}_2]^-$ Cluster Anion

Passing to $[\text{ClO}_2\cdot\text{Na}\cdot\text{ClO}_2]^-$ cluster ion, the reactive channels reported in Scheme 2 have been observed from the reaction with SO_2 . The identity of the ionic products from Reactions (6)–(11) have been probed by collision–induced dissociation experiments as discussed below.

The reaction of $[\text{ClO}_2\cdot\text{Na}\cdot\text{ClO}_2]^-$ with SO_2 at 298 K is fast and efficient showing an overall rate constant (k_{dec}) of 7.48×10^{-10} ($\pm 30\%$) $\text{cm}^3 \text{s}^{-1} \text{mol}^{-1}$ at 298 K. This value is only 0.82 times lower than the corresponding one for the bare ClO_2^- species, whereas the efficiencies (k/k_{coll}) of the two processes are similar (66.0% vs. 63.8%, Table 1). The intrinsic reactivity of the $[\text{ClO}_2\cdot\text{Na}\cdot\text{ClO}_2]^-$ anion towards SO_2 is comparable to that of the $[\text{Cl}\cdot\text{Na}\cdot\text{ClO}_2]^-$ species, as demonstrated by rather close branching ratios for the three reaction pathways (Table 1). Nonetheless, the concomitant presence of two reactive ClO_2^- moieties in the $[\text{ClO}_2\cdot\text{Na}\cdot\text{ClO}_2]^-$ ion gives rise to an intricate reaction picture as shown in the above Scheme 2 and in the kinetic plot of Figure 4.



Scheme 2. Reactivity scheme $[\text{ClO}_2 \cdot \text{Na} \cdot \text{ClO}_2]^-$ ions ($m/z = 157$) with SO_2 . Oxygen transfer channels (OIT, OAT, DOT) and bimolecular rate constants are indicated for each reaction.

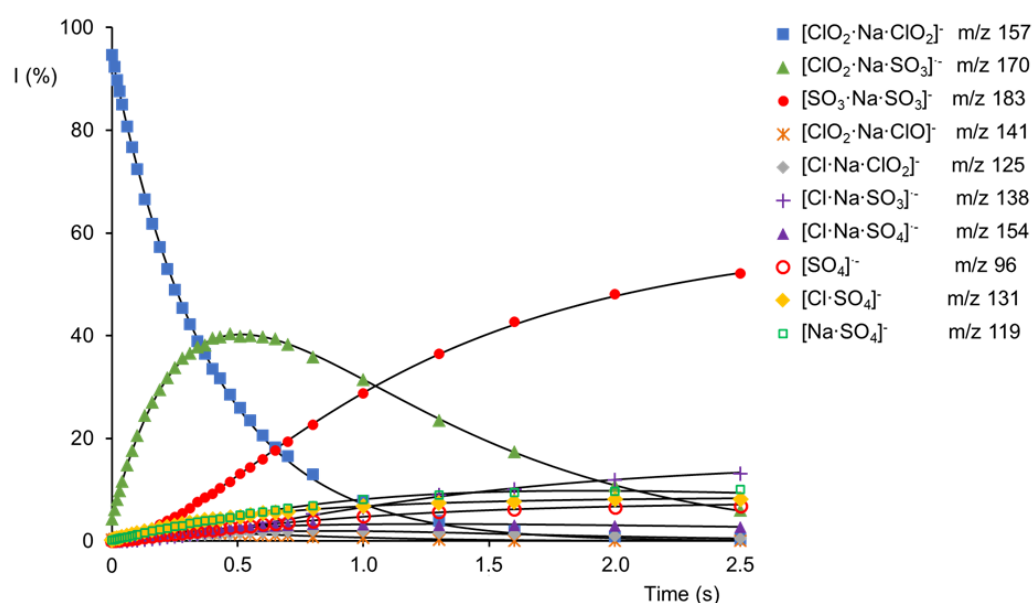


Figure 4. Kinetic plot and best fit lines of the reaction of isolated $[\text{NaClO}_2 \cdot \text{ClO}_2]^-$ ions ($m/z = 157$) with SO_2 . $P(\text{SO}_2) = 3.30 \times 10^{-7}$ Torr. ■ $[\text{ClO}_2 \cdot \text{Na} \cdot \text{ClO}_2]^-$ ($m/z = 157$) ($R^2 = 0.9991$); ▲ $[\text{ClO}_2 \cdot \text{Na} \cdot \text{SO}_3]^-$ ($m/z = 170$) ($R^2 = 0.9986$); ● $[\text{SO}_3 \cdot \text{Na} \cdot \text{SO}_3]^-$ ($m/z = 183$) ($R^2 = 0.9998$); × $[\text{ClO}_2 \cdot \text{Na} \cdot \text{ClO}]^-$ ($m/z = 141$) ($R^2 = 0.9888$); ◆ $[\text{Cl} \cdot \text{Na} \cdot \text{ClO}_2]^-$ ($m/z = 125$) ($R^2 = 0.9965$); + $[\text{Cl} \cdot \text{Na} \cdot \text{SO}_3]^-$ ($m/z = 138$) ($R^2 = 0.9967$); ▲ $[\text{Cl} \cdot \text{Na} \cdot \text{SO}_4]^-$ ($m/z = 154$) ($R^2 = 0.9912$); ○ $[\text{SO}_4]^-$ ($m/z = 96$) ($R^2 = 0.9946$); ◆ $[\text{Cl} \cdot \text{SO}_4]^-$ ($m/z = 131$) ($R^2 = 0.9992$); □ $[\text{Na} \cdot \text{SO}_4]^-$ ($m/z = 119$) ($R^2 = 0.9971$).

The main reaction of $[\text{ClO}_2 \cdot \text{Na} \cdot \text{ClO}_2]^-$ ion at $m/z = 157$ leads to the ionic product at $m/z = 170$, attributed to $[\text{ClO}_2 \cdot \text{Na} \cdot \text{SO}_3]^-$, and a $\text{ClO} \cdot$ radical species (Equation (6)). The CID mass spectrum of the ionic product at $m/z = 170$ shows a major dissociation into SO_3^- , which accounts for a $[\text{ClO}_2 \cdot \text{Na} \cdot \text{SO}_3]^-$ structure (Figure S7). As in the case of Cl-clustered species $[\text{Cl} \cdot \text{Na} \cdot \text{ClO}_2]^-$, the main reaction of $[\text{ClO}_2 \cdot \text{Na} \cdot \text{ClO}_2]^-$ consists of an oxygen ion transfer, resulting in a fast intracuster oxidation of SO_2 . The rate constant k_6 is 6.26×10^{-10} ($\pm 30\%$) $\text{cm}^3 \text{s}^{-1} \text{mol}^{-1}$ (Table 3), and a branching ratio of 81.8% (Table 1). The intracuster formation of SO_3^- gives rise to a negatively charged product in which one of the two ClO_2^- moieties only played a spectator role, whereas the sodium cation is reasonably involved in the coordination of the ClO_2^- and SO_3^- anions. However, the presence of a residual ClO_2^- moiety in the product ion $[\text{ClO}_2 \cdot \text{Na} \cdot \text{SO}_3]^-$ is responsible for the consecutive reactivity of this species, which is deeply discussed in the next paragraph (vide

infra). The complete reactive scheme of $[\text{ClO}_2\cdot\text{Na}\cdot\text{ClO}_2]^-$, integrated with the reactivity of $[\text{ClO}_2\cdot\text{Na}\cdot\text{SO}_3]^-$, is reported in the Supplementary Materials (Scheme S1), showing the complex and intricate reactivity of an only apparently simple species.

Table 3. Rate constants ($\text{cm}^3 \text{mol}^{-1} \text{s}^{-1}$) for the reaction: $[\text{ClO}_2\cdot\text{Na}\cdot\text{ClO}_2]^- + \text{SO}_2$. Only the most relevant rate constants are reported. OIT: oxygen ion transfer; OAT: oxygen atom transfer; DOT: double oxygen transfer; add: addition reaction.

Reactivity	$k \times 10^{-10} \text{ cm}^3 \text{ mol}^{-1} \text{ s}^{-1} \text{ §}$			
OIT	k_6			
	6.26			
OAT	k_7	$k_{7,1}$		
	0.364	9.57		
DOT	k_8	k_9	k_{10}	k_{11}
	0.251	0.417	0.134	0.222
SO ₂ add	k_{SO_2}			
	0.574			

§ $\pm 30\%$.

A second path, indeed a minor one, leads to an ionic product at m/z 141 and SO_3 (Equation (7)), formed through an OAT from one of the two ClO_2^- unit to SO_2 . The branching ratio is only 4.8% (Table 1) and a rate constant k_7 of $3.64 \times 10^{-11} (\pm 30\%) \text{ cm}^3 \text{ s}^{-1} \text{ mol}^{-1}$ (Table 3). The ionic product at m/z 141, resembles an aggregate in which a ClO_2^- anion and a ClO^- reactive moiety are both coordinated to sodium cation, although its fragmentation into the ClO_3^- species at m/z 83 seems to account for a $[\text{Cl}\cdot\text{Na}\cdot\text{ClO}_3]^-$ structure (Figure S8). Nonetheless, the $[\text{Cl}\cdot\text{Na}\cdot\text{ClO}_3]^-$ ion obtained by spraying a $\text{NaCl}/\text{NaClO}_3$ (1:1) millimolar solution resulted to be not reactive towards SO_2 (Figure S9).

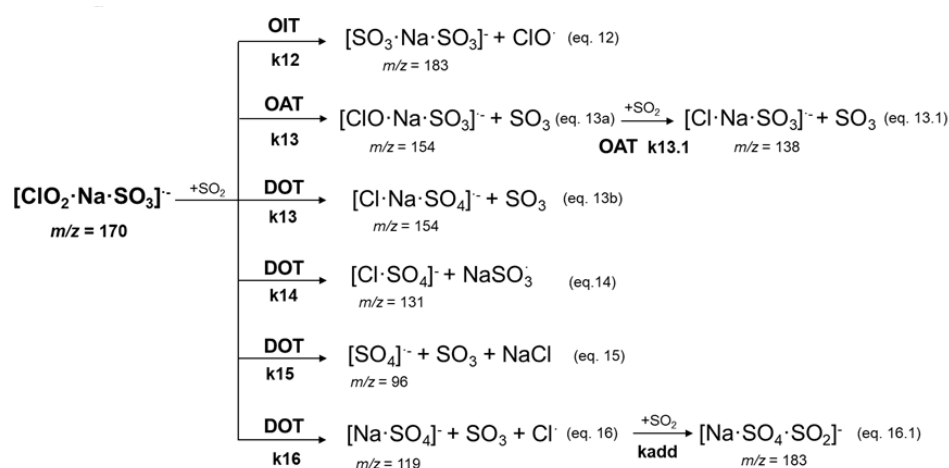
Therefore, it seems more likely to attribute the $[\text{ClO}\cdot\text{Na}\cdot\text{ClO}_2]^-$ connectivity to the ion at m/z 141 that rearranges to $[\text{Cl}\cdot\text{Na}\cdot\text{ClO}_3]^-$ upon CID, thus demonstrating the interaction of sodium cation with the ClO_2^- and ClO^- anions, rather than Cl^- and ClO_3^- species. The presence of two potential reactive units, ClO and ClO_2 , make the $[\text{ClO}\cdot\text{Na}\cdot\text{ClO}_2]^-$ cluster ion quite reactive. The consecutive OAT process observed (Equation (7.1)) has a rate constant $k_{7,1}$ of $9.57 \times 10^{-10} (\pm 30\%) \text{ cm}^3 \text{ s}^{-1} \text{ mol}^{-1}$ (Table 3), which is much higher than k_7 relative to the similar OAT process in Equation (7). Again, as for reactions 2 and 2.1, the reason lies in the different reactivity of the free chlorite and hypochlorite anions, the first undergoing faster OIT and the second faster OAT processes. The product ion at m/z 125 corresponds to the $[\text{Cl}\cdot\text{Na}\cdot\text{ClO}_2]^-$ species, as demonstrated by its characteristic fragmentation pattern and the distinctive reactivity discussed in the previous paragraph (Figures S10 and S11).

Four different DOT channels were reported for the $[\text{ClO}_2\cdot\text{Na}\cdot\text{ClO}_2]^-$ parent ion. The first three pathways (Equations (8)–(10)) resemble those already described for the $[\text{Cl}\cdot\text{Na}\cdot\text{ClO}_2]^-$ ion (Equations (3)–(5)), as the same product ions at m/z 154, 131, and 96 are respectively detected. The intracuster DOT processes reported in Equations (3) and (8) occurs with similar rate constants k_3 and k_8 , regardless the ligand $[\text{NaCl}]$ or $[\text{NaClO}_2]$ attached to the ClO_2^- moiety ($k_3 = 3.06$ vs. $k_8 = 2.51 \times 10^{-11} \text{ cm}^3 \text{ s}^{-1} \text{ mol}^{-1}$). A significantly faster formation of the $[\text{Cl}\cdot\text{SO}_4]^-$ ion at m/z 131 was reported for the $[\text{ClO}_2\cdot\text{Na}\cdot\text{ClO}_2]^-$ parent species with respect to $[\text{Cl}\cdot\text{Na}\cdot\text{ClO}_2]^-$ ($k_9 = 4.17$ vs. $k_4 = 1.47 \times 10^{-11} \text{ cm}^3 \text{ s}^{-1} \text{ mol}^{-1}$). Again, the formation of the free $[\text{SO}_4]^-$ product ion represents the lowest DOT process ($k_{10} = 1.34 \times 10^{-11} \text{ cm}^3 \text{ s}^{-1} \text{ mol}^{-1}$). In addition, a fourth DOT channel was observed only for the $[\text{ClO}_2\cdot\text{Na}\cdot\text{ClO}_2]^-$ parent ion which is worthy of note. In this case, the oxidation of SO_2 leads to the product at m/z 119 with a rate constant k_{11} of $2.22 \times 10^{-11} \text{ cm}^3 \text{ s}^{-1} \text{ mol}^{-1}$ (Equation (11)) which subsequently adds a further SO_2 molecule with a k_{add} of $5.74 \times 10^{-11} \text{ cm}^3 \text{ s}^{-1} \text{ mol}^{-1}$ (Equation (11.1), Table 3). Although the structure of the ionic species at m/z 119 could not be directly probed owing to its unproductive CID, a possible $[\text{Na}\cdot\text{SO}_4]^-$ formula can be reasonably supposed. The corresponding ion at m/z 119 was

also obtained by electrospraying a solution of Na_2SO_4 which, once isolated and reacted with SO_2 , gave a ligated $[\text{Na}\cdot\text{SO}_4\cdot\text{SO}_2]^-$ addition product with a rate constant consistent with k_{add} of Equation (11.1), thus confirming the identity of the parent species at m/z 119 (Figure S12). The $[\text{Na}\cdot\text{SO}_4]^-$ formula accounts for the oxidation of the sulphur atom of sulphur dioxide and the eventual reduction of the chlorine atoms of the $[\text{ClO}_2\cdot\text{Na}\cdot\text{ClO}_2]^-$ ion. Both the ClO_2^- units may be involved in the reaction, in which each ClO_2^- anion transfers an O^- moiety to SO_2 giving rise to an SO_4^{2-} species and the release of two ClO^- radicals. This hypothesis was confirmed by replacing one of the two ClO_2^- anions with the similarly oxygenated, but intrinsically unreactive ClO_3^- anion to obtain the $[\text{ClO}_3\cdot\text{Na}\cdot\text{ClO}_2]^-$ parent ion. When exposed to SO_2 , this species shows an intrinsic reactivity comparable to that of the $[\text{ClO}_2\cdot\text{Na}\cdot\text{ClO}_2]^-$ ion with the only exception of the product at m/z 119 that was not observed, thus highlighting the involvement of both ClO_2^- anions in the double O^- transfer.

2.3. Reactivity of $[\text{SO}_3\cdot\text{Na}\cdot\text{ClO}_2]^-$ Cluster Anion

To better investigate the consecutive reactivity of the product ion at m/z 170, arising from the $[\text{ClO}_2\cdot\text{Na}\cdot\text{ClO}_2]^-$ parent species through Equation (6), the putative $[\text{ClO}_2\cdot\text{Na}\cdot\text{SO}_3]^-$ ion was isolated from the sequence 157 to 170 (MS^2 -isolated) and separately reacted with SO_2 . The reactivity observed is illustrated in Scheme 3.



Scheme 3. Reactivity scheme $[\text{ClO}_2\cdot\text{Na}\cdot\text{SO}_3]^-$ ions ($m/z = 170$) with SO_2 . Oxygen transfer channels (OIT, OAT, DOT) and bimolecular rate constants are indicated for each reaction.

The overall reaction shows a rate constant (k_{dec}) of $3.74 \times 10^{-10} (\pm 30\%) \text{ cm}^3 \text{ s}^{-1} \text{ mol}^{-1}$ and an efficiency of 33.0% at 298 K (Table 1). These values agree with those reported for the other $[\text{X}\cdot\text{Na}\cdot\text{ClO}_2]^-$ parent species analysed and having a unique ClO_2^- reactive moiety (Table 1). Regarding, instead, the distribution of the three reaction paths, an even more pronounced increase of the DOT channels, accounting for a total amount of 22.7%, was observed (Table 1). The time progress of the reaction is described by the kinetic plot in Figure 5 and the rate constants of each pathway are reported in Table 4.

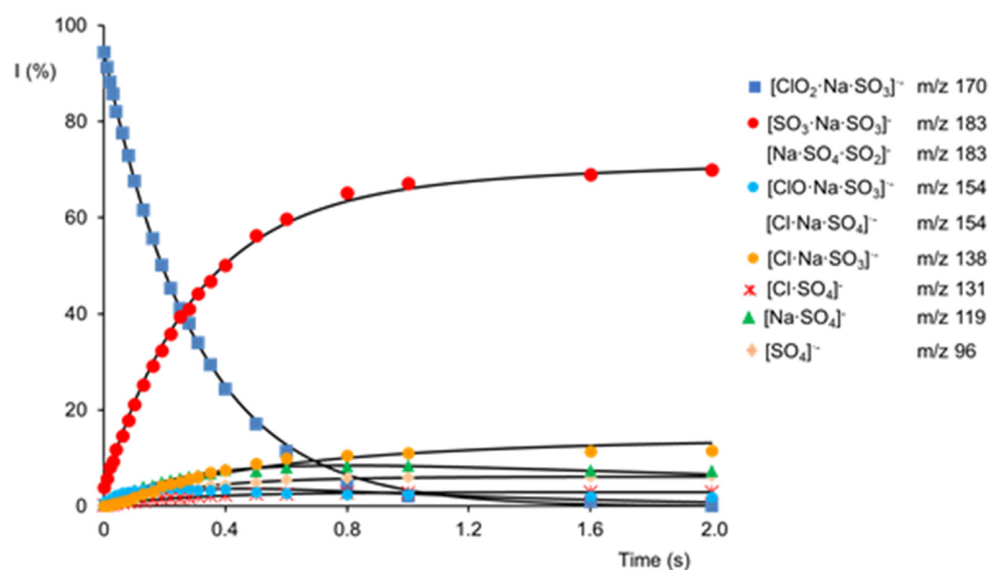


Figure 5. Kinetic plot and best fit lines of the reaction of isolated $[\text{ClO}_2\cdot\text{Na}\cdot\text{SO}_3]^-$ ions ($m/z = 170$) with SO_2 . $P_{\text{SO}_2} = 2.60 \times 10^{-7}$ Torr. ■ $[\text{ClO}_2\cdot\text{Na}\cdot\text{SO}_3]^-$ ($m/z = 170$) ($R^2 = 0.9991$); ● $[\text{SO}_3\cdot\text{Na}\cdot\text{SO}_3]^- / [\text{Na}\cdot\text{SO}_4\cdot\text{SO}_2]^-$ ($m/z = 183$) ($R^2 = 0.9986$); ● $[\text{ClO}\cdot\text{Na}\cdot\text{SO}_3]^- / [\text{Cl}\cdot\text{Na}\cdot\text{SO}_4]^-$ ($m/z = 154$) ($R^2 = 0.9686$); ● $[\text{Cl}\cdot\text{Na}\cdot\text{SO}_3]^-$ ($m/z = 138$) ($R^2 = 0.9880$); × $[\text{Cl}\cdot\text{SO}_4]^-$ ($m/z = 131$) ($R^2 = 0.9950$); ▲ $[\text{Na}\cdot\text{SO}_4]^-$ ($m/z = 119$) ($R^2 = 0.9973$); ◆ $[\text{SO}_4]^-$ ($m/z = 96$) ($R^2 = 0.9946$).

Table 4. Rate constants ($\text{cm}^3 \text{mol}^{-1} \text{s}^{-1}$) for the reaction $[\text{ClO}_2\cdot\text{Na}\cdot\text{SO}_3]^- + \text{SO}_2$. Only the most relevant rate constants are reported. OIT: oxygen ion transfer; OAT: oxygen atom transfer; DOT: double oxygen transfer; add: addition reaction.

Reactivity	$k \times 10^{-10} \text{ cm}^3 \text{ mol}^{-1} \text{ s}^{-1} \S$		
OIT	k_{12} 2.63		
OAT	k_{13} 0.260	$k_{13.1}$ 1.09	
DOT	k_{14} 0.167	k_{15} 0.222	k_{16} 0.457
SO_2 add	k_{add} 0.494		

§ $\pm 30\%$.

The intracluster OIT process (Equation (12)) proceeds quickly, showing a k_{12} of 2.63×10^{-10} ($\pm 30\%$) $\text{cm}^3 \text{s}^{-1} \text{mol}^{-1}$ (Table 4) and leading to the formation of an ion at m/z 183. Unfortunately, the CID mass spectrum of this species does not allow to distinguish between a $[\text{SO}_3\cdot\text{Na}\cdot\text{SO}_3]^-$ or a $[\text{Na}\cdot\text{SO}_4\cdot\text{SO}_2]^-$ structure (Figure S14), the latter already observed as a product of the DOT process involving the $[\text{ClO}_2\cdot\text{Na}\cdot\text{ClO}_2]^-$ parent ion. Nonetheless, based on the reactivity of naked ClO_2^- and knowing that the SO_3^- moiety is notoriously unreactive with SO_2 , it is reasonable to suppose a $[\text{SO}_3\cdot\text{Na}\cdot\text{SO}_3]^-$ general formula for this species.

The $[\text{ClO}_2\cdot\text{Na}\cdot\text{SO}_3]^-$ parent ion is also involved in an OAT reaction proceeding with a k_{13} of 2.60×10^{-11} ($\pm 30\%$) $\text{cm}^3 \text{s}^{-1} \text{mol}^{-1}$ and giving rise to an ion at m/z 154 that is consistent with a $[\text{ClO}\cdot\text{Na}\cdot\text{SO}_3]^-$ structure. The consecutive OAT reactivity of this species leading to the ion at m/z 138 (Equation (13.1); $k_{13.1} = 1.09 \times 10^{-10}$ ($\pm 30\%$) $\text{cm}^3 \text{s}^{-1} \text{mol}^{-1}$, Table 4, Figure S11) accounts for the presence of the surrounding reactive ClO^- moiety in $[\text{ClO}\cdot\text{Na}\cdot\text{SO}_3]^-$ ($m/z = 154$). When MS^3 -isolated into the ion trap by the sequence 170 to 154 and exposed to SO_2 , the ionic species at m/z 154 is only partially reactive towards this neutral gas. A portion of the ionic population at m/z 154 survives

over time, hinting at the concomitant presence of the unreactive $[\text{Cl}\cdot\text{Na}\cdot\text{SO}_4]^-$ species together with the $[\text{ClO}\cdot\text{Na}\cdot\text{SO}_3]^-$ isobaric ion that is consumed in the consecutive reaction (Figure S15). The $[\text{Cl}\cdot\text{Na}\cdot\text{SO}_4]^-$ species can reasonably arise from a direct intracuster DOT channel (Equation (13b)), as previously observed in analogous processes involving the $[\text{Cl}\cdot\text{Na}\cdot\text{ClO}_2]^-$ and $[\text{ClO}_2\cdot\text{Na}\cdot\text{ClO}_2]^-$ parent ions (Equations (3) and (8)). As a result, the O_2^- transfer from ClO_2^- to SO_2 triggers the release of a neutral SO_3 moiety according to the electron affinity values of the species involved in the reaction [27–34,65]. Unfortunately, it was not possible to independently measure k_{13b} , which is therefore included with that of the OAT transfer, k_{13} . As a consequence, the branching ratio of the OAT might be slightly overestimated, at the expense of that for the DOT process, which could therefore be underestimated. Two other DOT pathways reported in Equations (14) and (15) were also previously observed for the $[\text{Cl}\cdot\text{Na}\cdot\text{ClO}_2]^-$ and $[\text{ClO}_2\cdot\text{Na}\cdot\text{ClO}_2]^-$ parent clusters (Equations (4) and (9), Equations (5) and (10)). All these pathways show rather similar formation rate constants of the $10^{-11} \text{ cm}^3 \text{ s}^{-1} \text{ mol}^{-1}$ order of magnitude (Table 4).

$[\text{ClO}_2\cdot\text{Na}\cdot\text{SO}_3]^-$ also reacts with SO_2 , leading to the $[\text{Na}\cdot\text{SO}_4]^-$ product ion at m/z 119 (Equation (16)). The reaction, showing a k_{16} of $4.57 \times 10^{-11} \text{ cm}^3 \text{ s}^{-1} \text{ mol}^{-1}$, proceeds with an intracuster O_2^- transfer. Such unusual reactivity probably involves both the ClO_2^- anion that triggers a classic O_2^- transfer and the SO_3^- moiety that may be responsible for an electron transfer, giving rise to an SO_4^{2-} anion through a concerted rearrangement. As previously reported (Equation (11.1)), the consecutive addition of an SO_2 molecule to the $[\text{Na}\cdot\text{SO}_4]^-$ product ion is observed, thus confirming the identity of the ion at m/z 119.

Finally, as to the reactivity of higher species such as $[(\text{NaClO}_2)_n\cdot\text{ClO}_2]^-$, only the rate constant relative to cluster with $n = 2$ has been measured (Table 1), which does not appear to be affected by the number of additional NaClO_2 units compared to $[\text{ClO}_2\cdot\text{Na}\cdot\text{ClO}_2]^-$. However, it was not possible to evaluate the branching ratio of the OIT, OAT and DOT processes of $[(\text{NaClO}_2)_2\cdot\text{ClO}_2]^-$, due to the low intensity signals relative to parent cluster ions, and to the complex array of peaks resulting from the reaction with SO_2 .

3. Materials and Methods

Mass spectrometric experiments were carried out on an LTQ-XL linear ion-trap mass spectrometer (Thermo Fisher Scientific) that was in-house modified to perform ion-molecule reactions (IMR) [53]. Water-acetonitrile (1:1) solutions of NaClO_2 at millimolar concentrations were injected into the ESI (electrospray ionization) source of the instrument at a flow rate of $5 \mu\text{L min}^{-1}$ via the on-board syringe pump and using nitrogen as sheath and auxiliary gas (flow rate = 11 and 2 arbitrary units respectively, a. u. $\sim 0.37 \text{ L min}^{-1}$). Other $[\text{ML}\cdot\text{ClO}_2]^-$ cluster anions ($\text{L} = \text{F}, \text{Br}, \text{I}, \text{ClO}_3$; $\text{M} = \text{Li}, \text{Na}$) investigated in this work were obtained from millimolar solutions of 1:1 ML and NaClO_2 salts dissolved in water-acetonitrile (1:1). To generate chlorite cluster ions and optimize the ion transmission, spray voltage was tuned in the 1.8–3.2 kV range, whereas the capillary temperature was set at 275 °C. The distribution of the ionic aggregates strictly depends on the capillary and tube lens voltage. Hence, these parameters were in turn optimized to increase the signal intensity of the parent ion under investigation.

Once generated, reagent ions were transferred to the vacuum region of the trap, mass-to-charge isolated and reacted with sulphur dioxide. Each reaction product was then mass selected by a further step of isolation, that is typical of MS^n experiments performed by Ion Trap mass spectrometers, and the consecutive reactivity of these species was probed towards SO_2 to unravel a complete reaction picture. Furthermore, the ionic reactants and products were structurally characterized by collision-induced dissociation (CID) experiments performed by increasing the energy of mass-selected ions in the presence of helium as collision gas (pressure of ca. 3×10^{-3} Torr). Depending on the species of interest, normalized collision energies ranging between 20% and 40% were typically applied with an activation time of 30 ms. Ions were isolated with a window of 1 m/z , and the Q value was optimized to ensure stable trapping fields for all the ionic species under investigation.

Sulphur dioxide was introduced into the trap through a deactivated fused silica capillary that enters the vacuum chamber from a 6.25 mm hole placed in the backside of the mass spectrometer. The pressure of the neutral gas was kept constant by a metering valve and measured by a Granville-Phillips Series 370 Stabil Ion Vacuum Gauge. Owing to the position of the Pirani gauge, the actual sulphur dioxide pressure was estimated after calibration of the pressure reading [66]. Typical pressures of SO₂ ranged between 1.1×10^{-7} and 8.0×10^{-7} Torr, the uncertainty was estimated to be $\pm 30\%$. The signals of the ionic reactant and products were monitored over time as a function of the neutral concentration and for each reaction time an average of 10 scan acquisitions was recorded. The normalized collision energy was set to zero and the activation *Q* value was optimized to ensure stable trapping fields for all the ions. Xcalibur 2.0.6 software was used to acquire all the displayed mass spectra.

All the reactions can be regarded as pseudo-first-order processes due to the excess of neutral gas relative to the reactant ion in the trap. DynaFit4 software package [67] was used to perform nonlinear least squares regression to simultaneously fit reactant and products concentration versus time. Experimental data from the kinetic analyses were fitted to a mathematical model consistent with the postulated reaction mechanism. To check the validity of the kinetic schemes, the obtained unimolecular rate constants were used to simulate the time progress of the reactions using the kinetic simulation function contained in DynaFit4. Bimolecular rate constants *k* (cm³ molecule⁻¹ s⁻¹) were obtained dividing the pseudo-first-order constants (s⁻¹) by the concentration of neutral reagent gas. The branching ratios between the three channels (OIT, OAT, DOT) were calculated from the constants of formation of the primary direct products for each reactive species. The reaction efficiency was calculated as the ratio of the bimolecular rate constant *k* to the collision rate constant (*k_{coll}*), according to the average dipole orientation (ADO) theory [68]. To ensure the accuracy of the *k* values, approximately 15 independent measurements for each precursor ion were performed on different days over a sevenfold neutral pressure range. The standard deviation in the fitting parameters of the kinetic modelling used is usually evaluated between 10–20%, whereas the uncertainty attached to the measurement of the neutral pressure is typically evaluated $\pm 30\%$.

4. Conclusions

Mass spectrometry has been used to elucidate the gas-phase reactivity of [NaL·ClO₂]⁻ cluster anions (L = ClO_{*x*}⁻ with *x* = 0–3) with sulphur dioxide. These charged species can be taken as simplified models of large-scale reactions occurring in solution or in the flue-gas desulphurization processes, which are accomplished by sodium chlorite solutions.

The kinetic analysis has shown that SO₂ was efficiently oxidised by oxygen atom transfer (OAT), oxygen ion transfer (OIT), and double oxygen transfer (DOT) respective to SO₃, SO₃⁻ and SO₄⁻. In the case of OIT and DOT processes, an intracuster reaction was observed, by which the oxidised ionic forms of SO₂, namely SO₃⁻ and SO₄⁻, remain within the cluster and are not released as a free species. The results here reported show that when ClO₂⁻ is ligated to a non-redox active molecule, the complexation leads to a moderate reduction in the rate of oxidation processes, without substantially influencing the branching ratio. This effect contrasts, but not surprisingly, with what is observed in solution, where dissolved salts increase the SO₂ capture by increasing ionic strength of the solutions. In the gas phase, the direct and strong interaction of the chlorite anion with the ligand is detrimental to the reaction rate. However, the effect of redox active ligands, metallic or metal-free, could be quite different, as suggested by the reactivity observed with [ClO₂·Na·ClO₂]⁻, in which the second reactive ClO₂⁻ moiety succeeds in increasing the rate of the oxidation. Therefore, the ligation with a redox active group, different from the chlorite one, could succeed in tuning the oxidation processes.

Supplementary Materials: The following are available online. Figure S1: Full-scan mass spectrum of a NaClO₂ salt solution; Figure S2: Ion-molecule reaction between isolated [Cl·Na·ClO₂][−] cluster ion and SO₂; Figure S3: CID mass spectrum of [Cl·Na·SO₃][−] ion at *m/z* 138; Figure S4: CID mass spectrum of [Cl·Na·SO₄][−] ion at *m/z* 154; Figure S5: CID mass spectrum of [Cl·SO₄][−] ion at *m/z* 131; Figure S6: ion-molecule reaction between isolated [ClO₂·Na·ClO₂][−] cluster ion at *m/z* 157 SO₂; Figure S7: CID mass spectrum of [ClO₂·Na·SO₃][−] product ion at *m/z* 170; Figure S8: CID mass spectrum of (a) [ClO·Na·ClO₂][−] product ion at *m/z* and (b) [Cl·Na·ClO₃][−] standard ion at *m/z* 141; Figure S9: mass spectrum of the ion-molecule reaction of (a) [ClO·Na·ClO₂][−] ion at *m/z* and (b) [Cl·Na·ClO₃][−] standard ion at *m/z* 141 towards SO₂; Figure S10: mass spectrum of the ion-molecule reaction between [Cl·Na·ClO₂][−] consecutive product ion at *m/z* 125, MSⁿ-isolated from the reaction sequence *m/z* 157 to *m/z* 141 to *m/z* 125 and SO₂; Figure S11: magnified plot of the kinetic reported in Figure 4; Figure S12: mass spectrum of the ion-molecule reaction of (a) [Na·SO₄][−] product ion at *m/z* 119, MSⁿ-isolated, and (b) [Na·SO₄][−] standard ion at *m/z* 119 towards SO₂; Figure S13: mass spectrum of the ion-molecule reaction between [ClO₂·Na·SO₃][−] product ion at *m/z* 170, MSⁿ-isolated from the reaction sequence *m/z* 157 to *m/z* 170 and SO₂; Figure S14: CID mass spectrum of product ion at *m/z* 183; Figure S15: ion-molecule reaction of (a) a mixed ionic population at *m/z* 154, MSⁿ-isolated from the reaction sequence *m/z* 157 to *m/z* 170 to *m/z* 159 and (b) [Cl·Na·SO₄][−] ion at *m/z* 154, MSⁿ-isolated from the reaction of [Cl·Na·ClO₂][−] reactant ion towards SO₂; Figure S16: mass spectrum of the ion-molecule reaction between [Na·SO₄][−] product ion at *m/z* 119 and SO₂; Scheme S1: Complete reaction sequences of [ClO₂·Na·ClO₂][−] ion at *m/z* 157 and of its product ion [ClO₂·Na·SO₃][−] ion at *m/z* 170.

Author Contributions: Conceptualization, A.T. and C.S.; methodology, A.T.; validation, A.T., F.P. and C.S.; Funding acquisition, G.d.P.; investigation C.S.; data curation, C.S.; Supervision G.d.P.; Visualization C.S.; writing—original draft preparation, A.T. and C.S.; writing—review and editing A.T., C.S., F.P. and G.d.P. All authors have read and agreed to the published version of the manuscript.

Funding: This research was funded by Sapienza Rome University “Progetti di Ateneo” (Projects n. RM11816428291DFF, RM11715C81A54060, AR21916B746C06BB). C.S. thanks the Dipartimento di Chimica e Tecnologie del Farmaco, Sapienza Rome University, for a post-doc position within the project Dipartimenti di Eccellenza-L. 232/2016.

Institutional Review Board Statement: Not applicable.

Informed Consent Statement: Not applicable.

Data Availability Statement: Not applicable.

Conflicts of Interest: The authors declare no conflict of interest.

Sample Availability: Samples are not available from the authors.

References

1. Lima, R.; Bachmann, R.T. Pollutant emissions from modern incinerators. *Int. J. Environ. Pollut.* **2002**, *18*, 336. [[CrossRef](#)]
2. Vehlow, J. Air pollution control systems in WtE units: An overview. *Waste Manag.* **2015**, *37*, 58–74. [[CrossRef](#)]
3. Muralikrishna, I.V.; Manickam, V. *Environmental Management*; Elsevier Inc.: Amsterdam, The Netherlands, 2017.
4. Seinfeld, J.H.; Pandis, S.N. *Atmospheric Chemistry and Physics: From Air Pollution to Climate Change*, 3rd ed.; John Wiley and Sons: New York, NY, USA, 2016.
5. Dupart, Y.; King, S.M.; Nekat, B.; Nowak, A.; Wiedensohler, A.; Herrmann, H.; David, G.; Thomas, B.; Miffre, A.; Rairoux, P.; et al. Mineral dust photochemistry induces nucleation events in the presence of SO₂. *Proc. Natl. Acad. Sci. USA* **2012**, *109*, 20842–20847. [[CrossRef](#)]
6. Directive (EU) 2016/2284 of the European Parliament and of the Council of 14 December 2016 on the Reduction of National Emissions of Certain Atmospheric Pollutants, Amending Directive 2003/35/EC and Repealing Directive 2001/81/EC.
7. Woodard & Curran, Inc. *Industrial Waste Treatment Handbook*, 2nd ed.; Elsevier Inc.: Amsterdam, The Netherlands, 2006.
8. Hu, G.; Dam-Johansen, K.; Wedel, S.; Peterhansen, J. Review of the direct sulfation reaction of limestone. *Prog. Energy Combust. Sci.* **2006**, *32*, 386–407. [[CrossRef](#)]
9. Koralegedara, N.H.; Pinto, P.X.; Dionysiou, D.; Al-Abed, S.R. Recent advances in flue gas desulfurization gypsum processes and applications—A review. *J. Environ. Manag.* **2019**, *251*, 109572. [[CrossRef](#)] [[PubMed](#)]
10. Zhao, Y.; Guo, T.; Chen, Z. Experimental study on simultaneous desulfurization and denitrification from flue gas with composite absorbent. *Environ. Prog. Sustain. Energy* **2010**, *30*, 216–220. [[CrossRef](#)]

11. Adewuyi, Y.G.; He, X.; Shaw, H.; Lolertpihop, W. Simultaneous absorption and oxidation of NO and SO₂ by aqueous solutions of sodium chlorite. *Chem. Eng. Commun.* **1999**, *174*, 21–51. [[CrossRef](#)]
12. Flagiello, D.; Di Natale, F.; Erto, A.; Lancia, A. Wet oxidation scrubbing (WOS) for flue-gas desulphurization using sodium chlorite seawater solutions. *Fuel* **2020**, *277*, 118055. [[CrossRef](#)]
13. Chu, H.; Chien, T.-W.; Twu, B.-W. The absorption kinetics of NO in NaClO₂/NaOH solutions. *J. Hazard. Mater.* **2001**, *B84*, 241–252. [[CrossRef](#)]
14. Chu, H.; Chien, T.-W.; Twu, B.-W. Simultaneous absorption of SO₂ and NO in a stirred tank reactor with NaClO₂/NaOH solutions. *Water Air Soil Pollut.* **2003**, *143*, 337–350. [[CrossRef](#)]
15. Pourmohammadbagher, A.; Jamshidi, E.; Ale-Ebrahim, H.; Dabir, S. Study on simultaneous removal of NO_x and SO₂ with NaClO₂ in a novel swirl wet system. *Ind. Eng. Chem. Res.* **2011**, *50*, 8278–8284. [[CrossRef](#)]
16. Chien, T.-W.; Chu, H. Removal of SO₂ and NO from flue gas by wet scrubbing using an aqueous NaClO₂ solution. *J. Hazard. Mater.* **2000**, *80*, 43–57. [[CrossRef](#)]
17. Krzyżyńska, R.; Zhao, Y.; Hutson, N. Absorption of NO_x, SO₂, and mercury in a simulated additive-enhanced wet flue gas desulphurization scrubber. *Polish J. Environ. Stud.* **2010**, *19*, 1255–1262.
18. Andreasen, A.; Mayer, S. Use of Seawater Scrubbing for SO₂ Removal from Marine Engine Exhaust Gas. *Energy Fuels* **2007**, *21*, 3274–3279. [[CrossRef](#)]
19. Byun, Y.; Hamilton, I.P.; Tu, X.; Shin, D.N. Formation of chlorinated species through reaction of SO₂ with NaClO₂ powder and their role in the oxidation of NO and Hg⁰. *Environ. Sci. Pollut. Res.* **2014**, *21*, 8052–8058. [[CrossRef](#)]
20. Coelho, F.; Eberlin, M.N. The bridge connecting gas-phase and solution chemistries. *Angew. Chem. Int. Ed.* **2011**, *50*, 5261–5263. [[CrossRef](#)]
21. Zhu, W.; Yuan, Y.; Zhou, P.; Zeng, L.; Wang, H.; Tang, L.; Guo, B.; Chen, B. The expanding role of electrospray ionization mass spectrometry for probing reactive intermediates in solution. *Molecules* **2012**, *17*, 11507–11537. [[CrossRef](#)]
22. Fabris, D. Mass spectrometric approaches for the investigation of dynamic processes in condensed phase. *Mass Spectrom. Rev.* **2004**, *24*, 30–54. [[CrossRef](#)]
23. Troiani, A.; Rosi, M.; Garzoli, S.; Salvitti, C.; de Petris, G. Iron-Promoted C-C Bond Formation in the Gas Phase. *Angew. Chem. Int. Ed.* **2015**, *54*, 14359–14362. [[CrossRef](#)]
24. Troiani, A.; De Petris, G.; Pepi, F.; Garzoli, S.; Salvitti, C.; Rosi, M.; Ricci, A. Base-Assisted Conversion of Protonated D-Fructose to 5-HMF: Searching for Gas-Phase Green Models. *ChemistryOpen* **2019**, *8*, 1190–1198. [[CrossRef](#)]
25. Vikse, K.L.; Ahmadi, Z.; Manning, C.C.; Harrington, D.A.; McIndoe, J.S. Powerful insight into catalytic mechanisms through simultaneous monitoring of reactants, products, and intermediates. *Angew. Chem. Int. Ed.* **2011**, *50*, 8304–8306. [[CrossRef](#)] [[PubMed](#)]
26. Gronert, S. Mass spectrometric studies of organic ion/molecule reactions. *Chem. Rev.* **2001**, *101*, 329–360. [[CrossRef](#)] [[PubMed](#)]
27. Domínguez, I.; Frenich, A.G.; Romero-González, R. Mass spectrometry approaches to ensure food safety. *Anal. Methods* **2020**, *12*, 1148–1162. [[CrossRef](#)]
28. Wang, X.; Wang, S.; Cai, Z. The latest developments and applications of mass spectrometry in food-safety and quality analysis. *Trends Anal. Chem.* **2013**, *52*, 170–185. [[CrossRef](#)]
29. Cimino, P.; Troiani, A.; Pepi, F.; Garzoli, S.; Salvitti, C.; Di Rienzo, B.; Barone, V.; Ricci, A. From ascorbic acid to furan derivatives: The gas phase acid catalyzed degradation of vitamin C. *Phys. Chem. Chem. Phys.* **2018**, *20*, 17132–17140. [[CrossRef](#)]
30. Geoghegan, K.F.; Kelly, M.A. Biochemical applications of mass spectrometry in pharmaceutical drug discovery. *Mass Spectrom. Rev.* **2005**, *24*, 347–366. [[CrossRef](#)]
31. Loos, G.; Van Schepdael, A.; Cabooter, D. Quantitative mass spectrometry methods for pharmaceutical analysis. *Philos. Trans. R. Soc. A Math. Phys. Eng. Sci.* **2016**, *374*, 20150366. [[CrossRef](#)]
32. Forte, G.; Chiarotto, I.; Giannicchi, I.; Loreto, M.A.; Martinelli, A.; Micci, R.; Pepi, F.; Rossi, S.; Salvitti, C.; Stringaro, A.; et al. Characterization of naproxen-polymer conjugates for drug-delivery. *J. Biomater. Sci. Polym. Ed.* **2015**, *27*, 69–85. [[CrossRef](#)]
33. Vestal, M.L. The Future of Biological Mass Spectrometry. *J. Am. Soc. Mass Spectrom.* **2011**, *22*, 953–959. [[CrossRef](#)]
34. Finehout, E.J.; Lee, K.H. An introduction to mass spectrometry applications in biological research. *Biochem. Mol. Biol. Educ.* **2004**, *32*, 93–100. [[CrossRef](#)]
35. de Laeter, J.R. Mass spectrometry and geochronology. *Mass Spectrom. Rev.* **1998**, *17*, 97–125. [[CrossRef](#)]
36. Petrie, S.; Bohme, D.K. Ions in space. *Mass Spectrom. Rev.* **2006**, *26*, 258–280. [[CrossRef](#)] [[PubMed](#)]
37. Cacace, F.; Cipollini, R.; De Petris, G.; Troiani, A. The impervious route to the elusive HOOO⁻ anion. *Int. J. Mass Spectrom.* **2003**, *228*, 717–722. [[CrossRef](#)]
38. Cacace, F.; de Petris, G.; Pepi, F.; Troiani, A. Direct experimental evidence for the H₂O⁺O₂⁻ charge transfer complex: Crucial support to atmospheric photonucleation theory. *Angew. Chem. Int. Ed.* **2000**, *39*, 367–369. [[CrossRef](#)]
39. Cacace, F.; de Petris, G.; Pepi, F.; Rosi, M.; Troiani, A. Ionization of ozone/chlorofluorocarbon mixtures in atmospheric gases: Formation and remarkable dissociation of [CHXYO₃]⁺ complexes (X = H, Cl, F; Y = Cl, F). *Chem. Eur. J.* **2000**, *6*, 2572–2581. [[CrossRef](#)]
40. Johnson, G.; Tyo, E.C.; Castleman, A.W. Cluster reactivity experiments: Employing mass spectrometry to investigate the molecular level details of catalytic oxidation reactions. *Proc. Natl. Acad. Sci. USA* **2008**, *105*, 18108–18113. [[CrossRef](#)] [[PubMed](#)]

41. Johnson, G.E.; Mitrić, R.; Bonačić-Koutecký, V.; Castleman, A. Clusters as model systems for investigating nanoscale oxidation catalysis. *Chem. Phys. Lett.* **2009**, *475*, 1–9. [CrossRef]
42. Schlangen, M.; Schwarz, H. Effects of ligands, cluster size, and charge state in gas-phase catalysis: A happy marriage of experimental and computational studies. *Catal. Lett.* **2012**, *142*, 1265–1278. [CrossRef]
43. Dietl, D.-C.N.; Troiani, A.; Schlangen, M.; Ursini, O.; Angelini, G.; Apeloig, Y.; de Petris, G.; Schwarz, H. Mechanistic Aspects of Gas-Phase Hydrogen-Atom Transfer from Methane to $[\text{CO}]^+$ and $[\text{SiO}]^+$: Why Do They Differ? *Chem. Eur. J.* **2013**, *19*, 6662–6669. [CrossRef]
44. Schlangen, M.; Schwarz, H. Probing elementary steps of nickel-mediated bond activation in gas-phase reactions: Ligand- and cluster-size effects. *J. Catal.* **2011**, *284*, 126–137. [CrossRef]
45. Vikse, K.L.; McIndoe, J.S. Mechanistic insights from mass spectrometry: Examination of the elementary steps of catalytic reactions in the gas phase. *Pure Appl. Chem.* **2015**, *87*, 361–377. [CrossRef]
46. Vikse, K.L.; Ahmadi, Z.; McIndoe, J.S. The application of electrospray ionization mass spectrometry to homogeneous catalysis. *Coord. Chem. Rev.* **2014**, *279*, 96–114. [CrossRef]
47. Troiani, A.; Rosi, M.; Salvitti, C.; de Petris, G. The oxidation of sulfur dioxide by single and double oxygen transfer paths. *ChemPhysChem* **2014**, *15*, 2723–2731. [CrossRef]
48. Stewart, I.I. Electrospray mass spectrometry: A tool for elemental speciation. *Spectrochim. Acta Part B* **1999**, *54*, 1649–1695. [CrossRef]
49. Hao, C.; March, R.E. Electrospray ionization tandem mass spectrometric study of salt cluster ions: Part 2 Salts of polyatomic acid groups and of multivalent metals. *J. Mass Spectrom.* **2001**, *36*, 509–521. [CrossRef] [PubMed]
50. Eberlin, M.N. Electrospray ionization mass spectrometry: A major tool to investigate reaction mechanisms in both solutions and the gas phase. *Eur. J. Mass Spectrom.* **2007**, *13*, 19–28. [CrossRef]
51. Castleman, A.W., Jr.; Keese, R.G. Gas-phase clusters: Spanning the states of matter. *Science* **1988**, *241*, 36–42. [CrossRef]
52. Bondybey, V.E.; Beyer, M.K. How many molecules make a solution? *Int. Rev. Phys. Chem.* **2002**, *21*, 277–306. [CrossRef]
53. Troiani, A.; Salvitti, C.; de Petris, G. Gas-phase reactivity of carbonate ions with sulphur dioxide: An experimental study of clusters reactions. *J. Am. Soc. Mass Spectrom.* **2019**, *30*, 1964–1972. [CrossRef]
54. Shaik, S.; Mandal, D.; Ramanan, S.S.D.M.R. Oriented electric fields as future smart reagents in chemistry. *Nat. Chem.* **2016**, *8*, 1091–1098. [CrossRef]
55. Yue, L.; Li, J.; Zhou, S.; Sun, X.; Schlangen, M.; Shaik, S.; Schwarz, H. Control of product distribution and mechanism by ligation electric field in the thermal activation of methane. *Angew. Chem. Int. Ed.* **2017**, *56*, 10219–10223. [CrossRef]
56. Geng, C.; Li, J.; Schlangen, M.; Shaik, S.; Sun, X.; Wang, N.; Weiske, T.; Yue, L.; Zhou, S.; Schwarz, H. Oriented external electric fields as mimics for probing the role of metal ions and ligands in the thermal gas-phase activation of methane. *Dalton Trans.* **2018**, *47*, 15271–15277. [CrossRef]
57. de Petris, G.; Cartoni, A.; Troiani, A.; Angelini, G.; Ursini, O. Water activation by SO_2^+ ions: An effective source of OH radicals. *PhysChemChemPhys* **2009**, *11*, 9976–9978. [CrossRef]
58. de Petris, G.; Troiani, A.; Rosi, M.; Angelini, G.; Ursini, O. Selective activation of C-Cl and C-F bonds by SO^+ radical cations: An experimental and computational study. *ChemPlusChem* **2013**, *78*, 1065–1072. [CrossRef]
59. Troiani, A.; Rosi, M.; Garzoli, S.; Salvitti, C.; de Petris, G. Vanadium hydroxide cluster ions in the gas phase: Bond-forming reactions of doubly-charged negative ions by SO_2 -promoted V-O activation. *Chem. Eur. J.* **2017**, *23*, 11752–11756. [CrossRef] [PubMed]
60. Troiani, A.; Rosi, M.; Garzoli, S.; Salvitti, C.; de Petris, G. Sulphur dioxide cooperation in hydrolysis reactions of vanadium oxide and hydroxide cluster dianions. *New J. Chem.* **2018**, *42*, 4008–4016. [CrossRef]
61. Troiani, A.; Rosi, M.; Garzoli, S.; Salvitti, C.; de Petris, G. Effective redox reactions by chromium oxide anions: Sulfur dioxide oxidation in the gas phase. *Int. J. Mass Spectrom.* **2018**, *436*, 18–22. [CrossRef]
62. Salvitti, C.; Rosi, M.; Pepi, F.; Troiani, A.; de Petris, G. Reactivity of transition metal dioxide anions MO_2^- ($M = \text{Co}, \text{Ni}, \text{Cu}, \text{Zn}$) with sulfur dioxide in the gas phase: An experimental and theoretical study. *Chem. Phys. Lett.* **2021**, *776*, 138555. [CrossRef]
63. E Bartmess, J.; Georgiadis, R. Empirical methods for determination of ionization gauge relative sensitivities for different gases. *Vacuum* **1983**, *33*, 149–153. [CrossRef]
64. Kuzmic, P. Program DYNAFIT for the Analysis of Enzyme Kinetic Data: Application to HIV Proteinase. *Anal. Biochem.* **1996**, *237*, 260–273. [CrossRef]
65. Bowers, M.T.; Su, T. *Interactions between Ions and Molecules*; Plenum Press: New York, NY, USA, 1975.
66. Van Berkel, G.J.; Kertesz, V. Using the Electrochemistry of the Electrospray Ion Source. *Anal. Chem.* **2007**, *79*, 5510–5520. [CrossRef] [PubMed]
67. Linstrom, P.J.; Mallard, W.G. (Eds.) *NIST Chemistry WebBook*; NIST Standard Reference Database Number 69; National Institute of Standards and Technology: Gaithersburg, MD, USA, 1997. Available online: <http://webbook.nist.gov> (accessed on 20 October 2021).
68. Tro, N.J. *Chemistry, International Edition*; Pearson Education Inc.: Upper Saddle River, NJ, USA, 2016; pp. 341–343.